

Origin of diffuse scattering in relaxor ferroelectrics

P. Ganesh,¹ E. Cockayne,² M. Ahart,¹ R. E. Cohen,¹ B. Burton,² Russell J. Hemley,¹ Yang Ren,³
Wenge Yang,³ and Z.-G. Ye⁴

¹*Geophysical Laboratory, Carnegie Institution of Washington, 5251 Broad Branch Road, Washington, D.C. 20015, USA*

²*Ceramics Division, Materials Science and Engineering Laboratory, National Institute of Standards and Technology, Gaithersburg, Maryland 20899, USA*

³*Advanced Photon Source, Argonne National Laboratory, Argonne, Illinois 60439, USA*

⁴*Department of Chemistry and 4D LABS, Simon Fraser University, Burnaby, British Columbia, Canada V5A 1S6*

(Received 17 November 2009; revised manuscript received 1 March 2010; published 5 April 2010)

High-pressure and variable temperature single-crystal synchrotron x-ray measurements combined with first principles based molecular-dynamics simulations were used to study diffuse scattering in the relaxor ferroelectric system $\text{PbSc}_{1/2}\text{Nb}_{1/2}\text{O}_3$. Constant temperature experiments show a pressure-induced transition to the relaxor phase, in which butterfly- and rod-shaped diffuse scattering occurs around the $\{h00\}$ and $\{hh0\}$ Bragg spots. Simulations qualitatively reproduce the observed diffuse scattering features as well as their pressure-temperature behavior and show that they arise from polarization correlations between chemically ordered regions, which in previous simulations were shown to behave as polar nanoregions. Simulations also exhibit radial diffuse scattering [elongated toward and away from $\mathbf{Q}=(000)$] that persists even in the paraelectric phase; consistent with previous neutron experiments on $\text{PbMg}_{1/3}\text{Nb}_{2/3}\text{O}_3$.

DOI: [10.1103/PhysRevB.81.144102](https://doi.org/10.1103/PhysRevB.81.144102)

PACS number(s): 77.80.-e, 61.43.Bn, 64.60.Ej, 77.84.Ek

I. INTRODUCTION

Single-crystal relaxors exhibit extraordinary electromechanical coupling and show great promise for ultrasonic transducer applications.¹ They have broad frequency and temperature dependent dielectric maxima, which in the special case of relaxor-ferroelectrics^{2,3} drops to a much lower value below the ferroelectric transition temperature (T_{FE}). The origin of the relaxor phase has been a topic of intense research for over a decade. From refractive index measurements, Burns *et al.*⁴ suggested that formation of polar clusters below a characteristic temperature, now called the Burns temperature (T_d),⁴ gives rise to dielectric dispersion, which was confirmed experimentally.⁵ These clusters are thought to be a few nanometers in size and are called polar nanoregions (PNRs).

Recent x-ray and neutron experiments show characteristic shapes of diffuse scattering in the relaxor phases of several lead based relaxors,^{6–10} shapes that are absent, or greatly diminished, in their paraelectric and ferroelectric phases. The essential observed features are anisotropic diffuse scattering patterns around the Bragg peaks along $\langle 110 \rangle$ -type directions. The ferroelectric phase shows weak streaks similar to those in BaTiO_3 and KNbO_3 , but rotated by 45° . The paraelectric phase only shows radial diffuse scattering.

Several hypotheses have been advanced to explain the characteristic shapes.^{7,11–13} All of these models invoke some sort of anisotropic feature, such as anisotropic strain, correlated atomic shifts, or domain boundaries to generate the experimentally observed diffuse scattering features. None of these models capture a relaxor phase or allow investigation of T or P dependence or the coupling between chemical and polar order; thus, e.g., none of them can explain radial scattering. Fitting the shapes of diffuse scattering features is not sufficient to uniquely determine the nature of the microstructural feature that give rise to them.

Incorporating realistic polarization fluctuations via first principles derived models provides a basis for clarifying the nature of the PNR in relaxors and experimental diffuse scattering observations provide a critical test for any theoretical model. Here, we clarify the microstructural origin of diffuse scattering features in the relaxor and the paraelectric phases of $\text{PbSc}_{1/2}\text{Nb}_{1/2}\text{O}_3$ (PSN) and related materials by combining single-crystal x-ray diffraction experiments and first principles based molecular-dynamics simulations.¹⁴ Qualitatively, our simulations reproduce all essential T and P variations in the diffuse scattering; quantitatively, however, the simulations fail to reproduce observed transition points, hence we compare experimental results to simulations at elevated pressures to access a region of the simulated T - P phase diagram in which there is a relatively large relaxor region.

II. EXPERIMENTS

A. Experimental details

X-ray diffraction was measured on single-crystal PSN at beamlines 11-ID-C (0.1077 Å) and 16-BMD (0.436926 Å) of the Advanced Photon Sources (Argonne National Laboratory). Single crystals of chemically disordered PSN were grown from high-temperature solutions using a mixture of PbO and B_2O_3 as solvent.¹⁶ A crystal with dimensions of $70 \times 70 \times 20 \mu\text{m}^3$ and oriented along (001) was loaded into a diamond-anvil cell (DAC) with Ne as the pressure medium. A ruby chip and a small grain of Au were also loaded for pressure determination (accuracy of 0.2 GPa). A MAR3450 image plate was used to record oscillation photographs. For low-temperature measurements, the DAC was loaded in a He flown cryostat, in which temperature was measured with a thermocouple to an accuracy of ± 2 K. Additional experimental details about beamline 11-ID-C and 16-BMD can be found in Refs. 17 and 18.

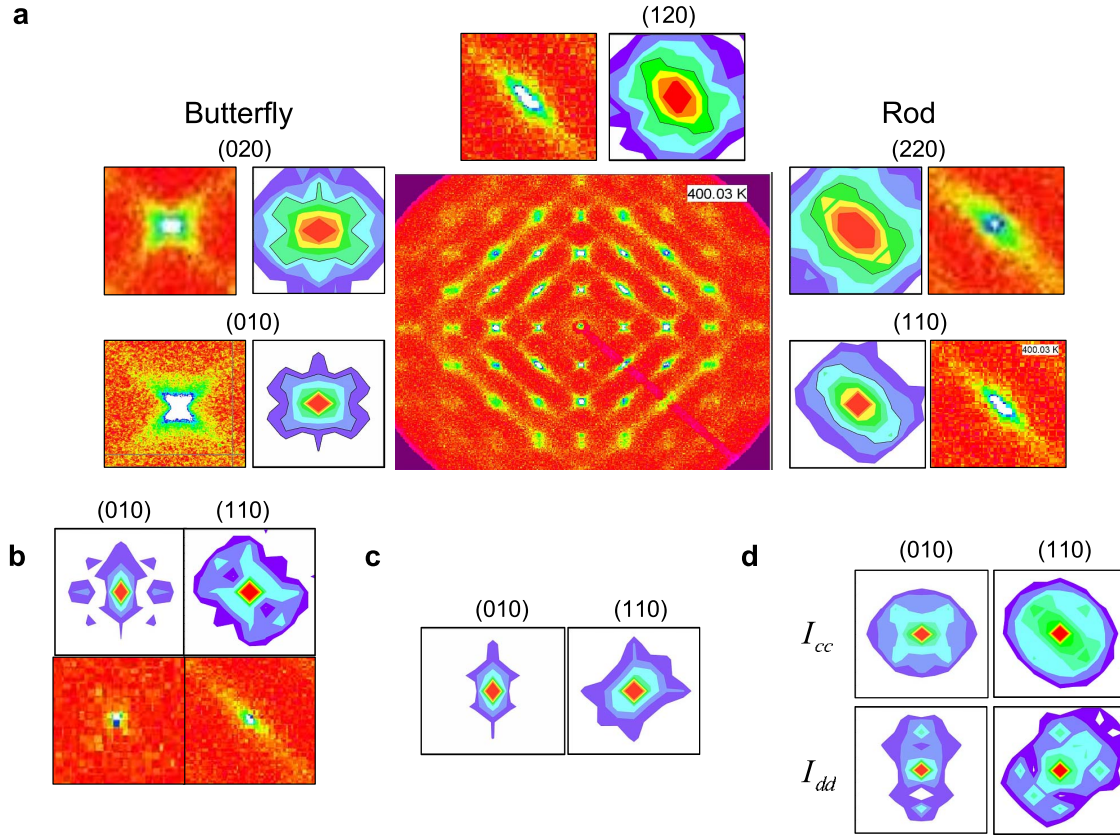


FIG. 1. (Color online) Temperature dependence of diffuse scattering in $(hk0)$ plane from x-ray diffraction at ambient pressure, experiments (red/dark background), and simulations at $P=18$ GPa (white background with intensity range $\{11,15\}$ in logarithmic scale) (a) Characteristic butterfly- and rod-shaped diffuse scattering [enhanced intensity along $[110]$ and $[1\bar{1}0]$ directions avoiding $\mathbf{Q}=(000)$] is observed in the relaxor phase around $\{h00\}$ and $\{hh0\}$ Bragg spots, respectively, in experiments (400 K) and simulations (200 K). (b) In the ferroelectric phase, the characteristic shapes diminish in experiments (250 K), similar to simulations (10 K). (c) In the paraelectric phase, simulations (320 K) only show radial diffuse scattering in good agreement with experiments (Ref. 15). (d) The partial contribution to the diffuse scattering from COR-COR correlations (I_{cc}) show the butterfly and rod shapes, while the partial contribution from CDR-CDR correlations (I_{dd}) show only the radial patterns in the simulated relaxor phase.

Single-crystal diffraction patterns were first measured at ambient pressure at various temperatures between 250 and 400 K. Temperature was subsequently decreased, and at each temperature of $T=300, 130,$ and 50 K, pressure was applied and x-ray data was collected. The applied pressure ranged from ambient pressure to 12 GPa.

Because of its (001) orientation in a cryostat, only the $(hk0)$ indexed Bragg peaks could be observed. In a DAC experiment performed in a cryostat only a small window is available to collect the diffracted x-rays. When pressure is applied, there is an additional possibility of the sample getting slightly reoriented. We measure the diffuse scattering around Bragg peaks indexed by a pseudocubic symmetry. We distinguish the ferroelectric, relaxor, and the paraelectric phases from their diffuse scattering features, which correlate with dielectric measurements for several relaxor materials.^{2,3} The small DAC-window opening caused the beam stop to deflect some of the direct beam onto the image plate resulting in a bright spot close to the center. To facilitate measurement of the diffuse scattering signal, the sample was rocked $\pm 6^\circ$ in omega.

B. Experimental results

On cooling at ambient pressure, PSN enters the relaxor phase below the Burns temperature [$T_d \sim 750$ K (Ref. 19)] and undergoes a ferroelectric transition at $T_{FE} \sim 365$ K. The average structure of the relaxor and the paraelectric phases is cubic, whereas the ferroelectric phase is rhombohedral. In our experiments at 400 K [Fig. 1(a)], we observe the characteristic butterfly- and rod-shaped diffuse scattering. At 250 K [Fig. 1(b)], below T_{FE} , the characteristic diffuse scattering diminishes considerably. Diffuse streaks connecting the Bragg peaks grow weaker yet persist in the ferroelectric phase, similar to those observed in BaTiO_3 and KNbO_3 (Ref. 20 and references therein).

We observe pressure induced phase transitions at 300 K, where around 1.4 GPa a reappearance of relaxor-phase diffuse scattering occurs; and persists up to 1.5 GPa but disappears at 1.8 GPa [Fig. 2(b)]. Disappearance of diffuse scattering at higher pressures indicates a relaxor to paraelectric phase transition, consistent with dielectric measurements.² At even higher pressures, one might expect a complete absence of the ferroelectric phase, with only the relaxor and paraelectric phases.

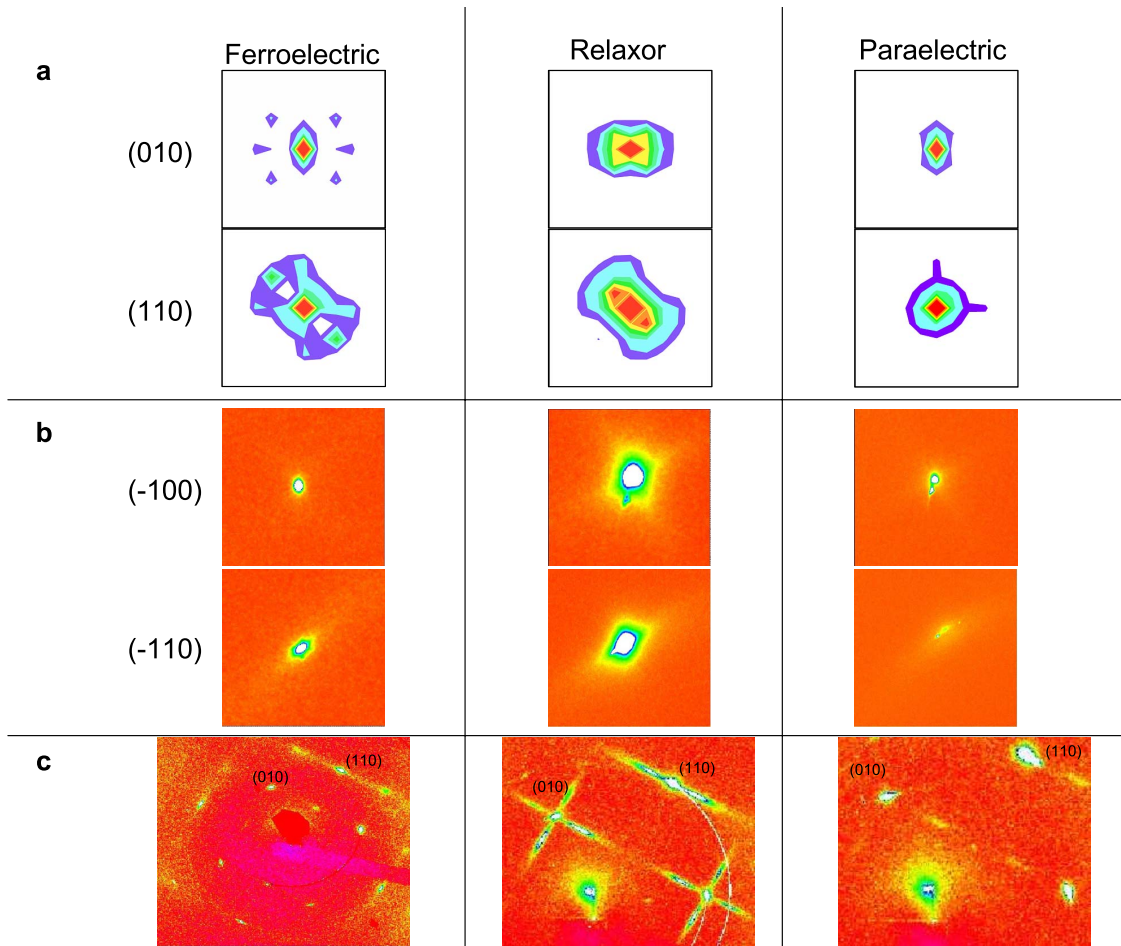


FIG. 2. (Color online) Pressure dependence of diffuse scattering in simulations at 180 K (white background) and experiments (red/dark background) in $(hk0)$ plane. (a) Simulated diffuse scattering in the ferroelectric ($P=14$ GPa), relaxor ($P=18$ GPa), and the paraelectric ($P=25$ GPa) phases, respectively, show characteristic relaxor-phase butterfly- and rod-shaped diffuse scattering and radial diffuse scattering in the pressure induced paraelectric phase. (b) Experiments at 300 K show weak diffuse scattering in the ferroelectric phase (ambient pressure) but strong butterfly- and rod-shaped scattering in the relaxor phase ($P=1.4$ GPa). In the paraelectric phase ($P=1.8$ GPa) the butterfly and rod shapes disappear. (c) At 50 K, we observe superlattice peaks in the ferroelectric phase ($P=0.6$ GPa). In the relaxor phase ($P=2.7$ GPa) on top of the butterfly and rod shapes we observe satellite spots. Further increase in pressure to 10 GPa destroys the diffuse scattering, leading to a pressure induced relaxor to paraelectric phase transition. (The bright spot near the center of the image is due to the beam stop.)

At 50 K [Fig. 2(b)] we also observe superlattice peaks at low pressures of $P=0.6$ GPa at $(h+1/2 \ k+1/2 \ 0)$ suggesting a reduction in symmetry; the intensities of these peaks diminish as increased pressure drives the system into the relaxor phase. Our experiments are on disordered PSN, hence the peaks are not due to chemical long-range order²¹ but may be due to octahedral rotations. In the relaxor phase, at 2.7 GPa, additional satellite peaks with diffuse wings emerge, and they persist up to 10 GPa. Our model, as discussed below, does not produce the satellite peaks or the superlattice peaks, indicating a different origin from the diffuse scattering shapes we explain below, such as long-range ordering of PNRs due to elastic interactions.

III. THEORY AND SIMULATIONS

A. Simulation details

We performed molecular-dynamics simulations using a model Hamiltonian obtained by expanding the potential en-

ergy of PSN about a high-symmetry perovskite reference structure and projecting onto the subspace of soft normal modes, dominated by Pb displacements, including the ferroelectric instabilities.^{22,23} Model parameters were fitted to first-principles density-functional calculations.²⁴ Molecular-dynamics simulations at each pressure-temperature were performed on a $40 \times 40 \times 40$ supercell that contained 32 000 atoms for about 300 ps with a time step of 0.6 fs using a Nose thermostat. The barostat only coupled to the homogeneous strain. Intensities were computed after an equilibration time of 150 ps.

The model has chemically ordered regions (CORs) with rock salt ordering of “Sc⁺³” and “Nb⁺⁵” B site ions, embedded in a chemically disordered region (CDR) that has a random B site configuration. This gives rise to a quenched random component to the local electric fields at the Pb sites. Relative to equal volumes of CDR, polarization is enhanced in CORs, thereby acting as PNRs.²⁴ The CORs are spatially

fixed because chemical order (disorder) is quenched, but their average polar orientations vary dynamically. [In the case of $\text{PbMg}_{1/3}\text{Nb}_{2/3}\text{O}_3$ (PMN), the CORs can be modeled by charge balanced random site ordering.²⁵ Simulations with such a COR model show relaxor features¹⁴ that are similar to those observed experimentally.] The model, thus, allows homogeneous strain to fluctuate; inhomogeneous strain higher-frequency phonon contributions to lattice polarization, and oxygen octahedral tilting are ignored.

Simulations of the PSN model exhibit ferroelectric, relaxor, and paraelectric phases depending on the temperature and pressure.¹⁴ The transition pressure decreases with temperature consistent with our experiments. Due to the inclusion of only a subset of the degrees of freedom and neglect of elastic interactions present in the real material, as well as errors in DFT, absolute values of pressure and temperature are expected to be different from those in experiments. We run simulations at elevated pressures to sample a larger relaxor field in the PT diagram. The different phases are identified by the cumulative histogram of the polarization in the chemically ordered regions.¹⁴ In the ferroelectric and paraelectric phases, the histogram is unimodal about nonzero and zero values, respectively. It shows a bimodal behavior with unequal peaks in the relaxor phase.

B. Scattering intensity and correlations

In x-ray and neutron-scattering experiments, the measured intensity is a Fourier transform of the ensemble averaged two-point density-density correlation.²⁶ Because the x-ray scattering factor of Pb is so much larger than that of Sc, Nb, or O, Pb displacements are expected to dominate the diffuse scattering from PSN; hence we restrict our detailed discussions of diffuse scattering to those from Pb displacements.

Assuming point particles, the intensity thus is $I(\mathbf{Q}) = \langle |\sum_i e^{i\mathbf{Q}\cdot\mathbf{r}_i}|^2 \rangle$, where i runs over the total number of Pb atoms in the supercell and \mathbf{Q} values commensurate with the supercell were chosen. Because the distribution of COR in our supercell is not entirely isotropic, we apply full cubic symmetry to the scattering intensity before comparing with experiments.

To understand the origin of the diffuse scattering *shapes*, we write the total intensity as a sum of Bragg and diffuse scattering and expand the latter in powers of $\xi_i = \mathbf{r}_i - \mathbf{R}_{0i}$, which is proportional to the local polarization and is a small quantity. The Bragg term is $\sum_{i,j} e^{i\mathbf{Q}\cdot(\mathbf{R}_{0i}-\mathbf{R}_{0j})}$, and the lowest order diffuse scattering term is

$$I_{diff}(\mathbf{G}, \mathbf{q}) = \left\langle \sum_{i,j} |\mathbf{G} + \mathbf{q}|^2 (\xi_i \cdot \hat{\alpha})(\xi_j \cdot \hat{\alpha}) \cos[\mathbf{Q} \cdot (\mathbf{R}_{0i} - \mathbf{R}_{0j})] \right\rangle, \quad (1)$$

where $\mathbf{q} = \mathbf{Q} - \mathbf{G}$ and \mathbf{G} is the Bragg spot. $\hat{\alpha}$ is the unit vector along $\mathbf{G} + \mathbf{q}$. The summation of pairs of atoms is equivalently rewritten as one over interatomic distances $\mathbf{R} = \mathbf{R}_{0i} - \mathbf{R}_{0j}$ so that Eq. (1) becomes the Fourier transform of projections of

real space displacement-displacement autocorrelation tensor $\vec{C}(\mathbf{R})$ along α :

$$I_{diff}(\mathbf{G}, \mathbf{q}) = \left\langle \sum_{\mathbf{R}} [\alpha \cdot \vec{C}(\mathbf{R}) \cdot \alpha] |\mathbf{Q}|^2 \cos(\mathbf{Q} \cdot \mathbf{R}) \right\rangle, \quad (2)$$

where $\vec{C}(\mathbf{R})$, given, in symmetric form is

$$C_{\alpha\beta}(\mathbf{R}) = \frac{1}{4} \sum_i (\xi_{i\alpha} \xi_{i\pm\mathbf{R}\beta} + \xi_{i\beta} \xi_{i\pm\mathbf{R}\alpha}), \quad (3)$$

and the “ \pm ” notation implies summation over both signs.

C. Simulation results and discussion

Figure 1 shows the temperature dependence of our computed diffuse pattern in the $(hk0)$ plane for the ferroelectric, relaxor, and the paraelectric phases at $P=18$ GPa. In the relaxor phase [Fig. 1(a)] we observe the characteristic butterfly and rod-shaped diffuse scattering around $(h00)$ and $(hh0)$ Bragg spots and spot intensities greatly diminish in the ferroelectric phase [Fig. 1(b)], in excellent agreement to experiments.

Pressure dependent changes in diffuse scattering [Fig. 2(a)] are similar to those induced by varying temperature. Again, our model yields qualitative agreement with experiment: greatly diminished diffuse scattering in the ferroelectric phase at low pressure; strong diffuse scattering in the relaxor phase at intermediate pressure; and only radial diffuse scattering in the high-pressure paraelectric phase. Experimentally observed streaks, like those in KNbO_3 are due to hopping between equivalent sites,²⁷ and superstructure peaks at 50 K may be due to octahedral rotations, both of which are excluded from our model. But these streaks are not characteristic of the relaxor phase, which is characterized by the butterfly- and rod-shaped scattering, that our simple model reproduces.

As the system is driven toward the paraelectric phase, by increasing temperature or pressure, the characteristic butterfly and rod shapes vanish; however, a weak diffuse pattern that extends radially toward and away from the origin [$\mathbf{Q}=(000)$] persists around all the Bragg peaks. Its intensity is larger in the direction away from the center than toward it, consistent with recent neutron experiments¹⁰ but absent in x-ray due to their low intensity. This is called radial diffuse scattering.⁶

To check for correlations in time the diffuse scattering was computed by averaging over different time segments. These averages do not change significantly during our simulation run time, which includes frequencies greater than 10 GHz. This suggests that only static (equal time) correlations cause diffuse scattering, consistent with recent experiments on PMN.¹⁰

We find the partial contributions to the scattering intensity from correlations due to atoms in the different regions (COR and CDR). These are shown in Fig. 1(d), where I_{cc} and I_{dd} are the intensities obtained by setting CDR and COR Pb displacements to zero, respectively. While I_{cc} shows characteristic rod and butterfly features, the radial diffuse pattern is absent. I_{dd} only shows the weak radial diffuse pattern. Thus,

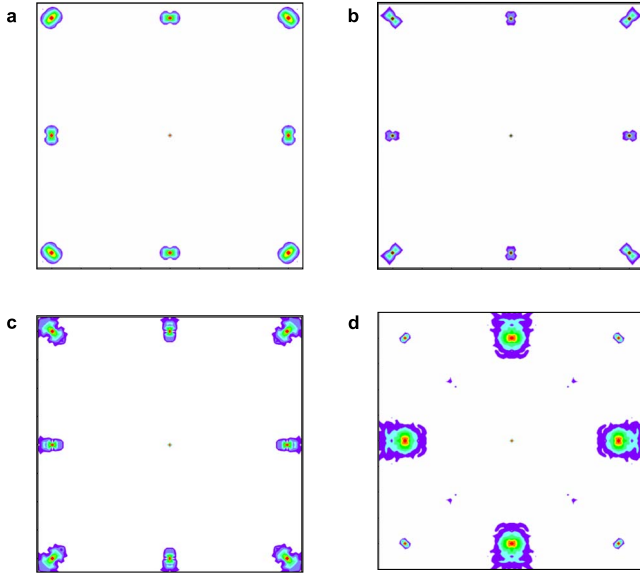


FIG. 3. (Color online) Simulated diffuse scattering results at $T=200$ K and $P=18$ GPa in $(hk0)$ plane. (a) Diffuse scattering from simulations with spherical CORs, i.e., no shape anisotropy, show butterfly- and rod-shaped features, suggesting that the details of shapes of CORs, which act as PNRs, are unimportant. (b) Diffuse scattering from a simulation with a single COR in a CDR matrix. Absence of butterfly- and rod-shaped diffuse scattering suggests that a single COR is not responsible for the observed diffuse scattering. (c) Diffuse scattering from a simulation with only CDR. Again, no butterfly- or rod-shaped scattering is observed. Rather radial scattering is seen and can hence be attributed to the chemically disordered region. (d) Diffuse scattering from polar oxygen displacements from the same simulation as in Fig. 1. Here the intensity range is $\{8,15\}$ in the logarithmic scale. Butterfly- and rod-shaped scattering is observed. The spatial extent of the scattering is smaller compared to those from Pb displacements.

it is the correlation between COR atoms that give rise to the characteristic diffuse patterns. The CDR Pb displacements are dominated by strong electric fields fixed in a quenched distribution of Sc and Nb atoms in the chemically disordered matrix, and therefore radial scattering persists even in the paraelectric phase. This is consistent with experimental observations on PMN.¹⁰ Note that our interpretation of radial diffuse scattering as being caused by chemical disorder differs from the interpretation of Gehring *et al.* in which it indicates chemical short-range order.¹⁰

Anisotropic shapes of PNRs (Ref. 7) and/or atomic shifts within a PNR (Refs. 11 and 13) have been proposed to give rise to the experimentally observed butterfly and rod-shaped diffuse scattering. Our simulations for which results are shown in Figs. 1 and 2 have CORs that are convex-polyhedron-shaped. In Fig. 3(a) we show our simulation results with all CORs chosen to be spherical, i.e., no shape anisotropy. We still observe the characteristic butterfly and rod shapes, suggesting that shapes of individual PNRs are not important. A single PNR would have ferroelectric atomic displacements. In Fig. 3(b) we show results of a single COR in a CDR matrix. We only observe the radial patterns, similar to our simulation results with no COR [Fig. 3(c)]. This is consistent with our earlier observation that it is the correla-

tion between CORs that yield the butterfly- and rod-shaped diffuse scattering whereas the CDR yields only radial diffuse scattering.

Oxygen displacements are expected to contribute significantly in neutron-scattering experiments.¹⁰ Although we do not have octahedral rotations, we do include oxygen displacements in the lowest energy polar mode. Figure 3(d) shows scattering only from the oxygen displacements. Note that the intensity range is now from 8 to 15 in the logarithmic scale. Butterfly- and rod-shaped diffuse scattering is obtained, but they have a smaller spread compared to those obtained from Pb displacements [Fig. 3(a)]. Further refinements of the model are needed to quantitatively determine the effect of oxygen displacements. We believe that it is the Pb displacements that are mainly responsible for the observed diffuse scattering in Pb-based relaxors. This is why we see the characteristic diffuse scattering even in our x-ray experiments which are dominated by scattering from Pb atoms.

In Eq. (1), for small $|\mathbf{q}|$, we approximate $\mathbf{G}+\mathbf{q}$ by \mathbf{G} and $\hat{\alpha}$ by the unit vector $\hat{\alpha}_{\mathbf{G}}$. Figure 4 shows the real space correlations in the relaxor phase (180 K, 18 GPa) with projections along $\hat{\alpha}_{\mathbf{G}}=[100]$ and $[110]$ summed over the z direction as well as their Fourier transforms. The diffuse scattering butterfly and rod shapes come from $\alpha_{\mathbf{G}}=[100]$ and $\alpha_{\mathbf{G}}=[110]$ projections, respectively, of the COR-COR real-space correlations. The CDR-COR regions have strong correlation along the direction perpendicular to the radial direction, leading to the radial diffuse scattering in Fourier space. In three-dimensional (3D) (not shown) the $[110]$ (as well as $[111]$) real space projections appear as ellipsoids, while the $[100]$ correlations appear as disks.

IV. CONCLUSIONS

We conclude that PSN shows ferroelectric \rightarrow relaxor \rightarrow paraelectric phase transitions with increasing temperature and/or pressure in our experiments. The relaxor phase in the experiments is characterized by butterfly- and rod-shaped diffuse scattering.

Simulations reveal that the anisotropic correlations from COR-COR Pb atoms, which only have displacive degrees of freedom, give rise to the characteristic relaxor-phase diffuse scattering. Polarization would be accompanied by local strain inhomogeneities that would cause additional contributions to the diffuse scattering,¹² but this is a *secondary* effect. The radial diffuse scattering is identified as coming from local concentration fluctuations at the B site, which cause corresponding fluctuations in local electric fields that induce Pb displacements. Because diffuse scattering comes from correlations in polar Pb displacements, we expect that they would be correlated with other quantities that are related to fluctuations in the local polarization, such as the dielectric constant, which will be presented elsewhere.

An increase in pressure reduces the ferroelectric well depth and therefore the ferroelectric Pb displacements in COR. This reduces PNR-PNR correlations (and not their sizes) and hence reduces the butterfly- and rod-shaped diffuse scattering. In the ferroelectric phase, the whole system,

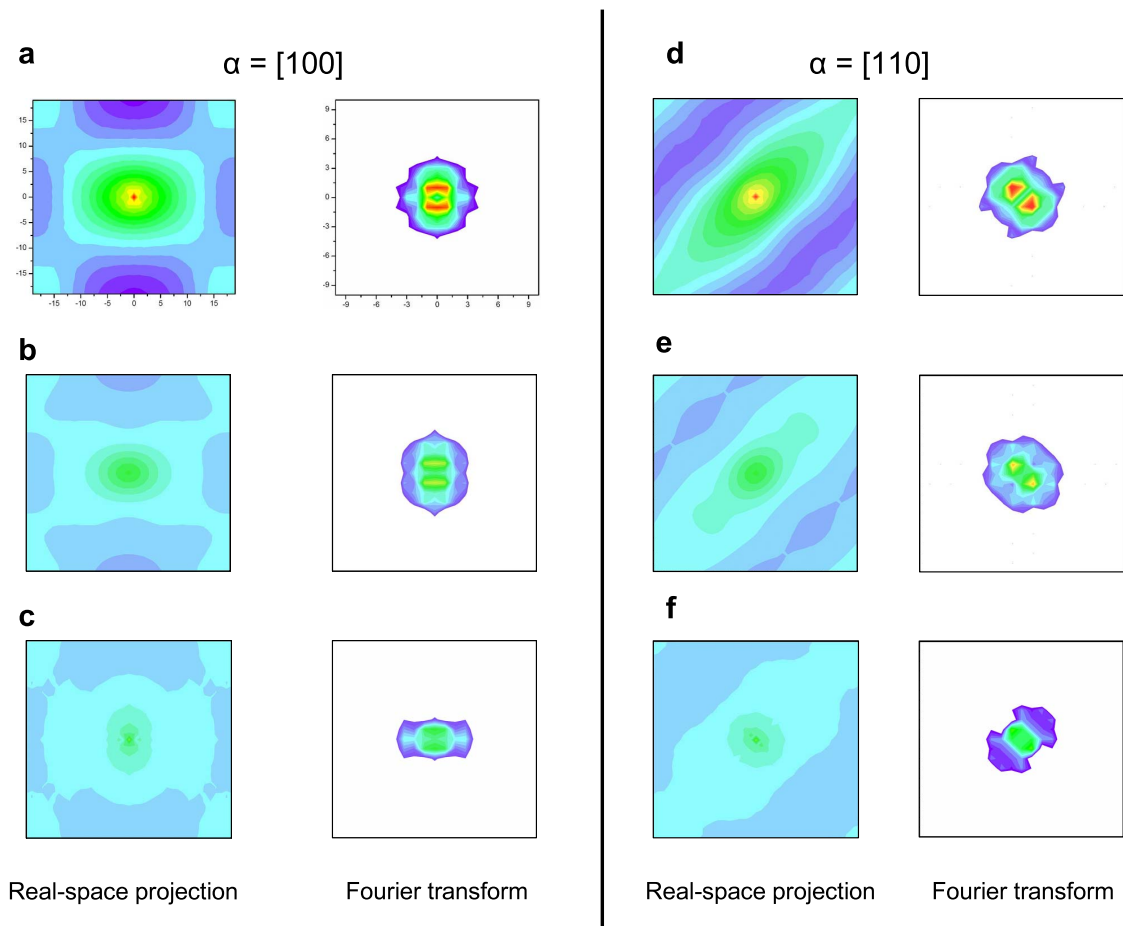


FIG. 4. (Color online) Real-space correlations [Eq. (3)] projected along $[100]$ and $[110]$ directions and their direct Fourier transforms. The real-space correlation figures have sides of length $40a$, where a is the lattice parameter and the Fourier-space is in units of $2\pi/40a$. (a) and (d) show correlations between all Pb atoms, which reproduce the experimentally observed butterfly- and rod-shaped diffuse scattering. (b) and (e) show the correlations between COR-COR regions which are extended in the real space along directions normal to the butterfly and rod directions. Their Fourier transform gives the characteristic diffuse scattering. (c) and (f) show the correlations between the CDR-CDR regions which when Fourier transformed give the radial patterns.

including the disordered matrix, has a uniform polarization along $\langle 111 \rangle$ directions. This enhancement of the average polarization reduces the typical deviation of the polarizations within COR from average, thus greatly diminishing the characteristic butterfly- and rod-shaped diffuse scattering features. With increase in temperature, thermal fluctuations of the polarization decrease the magnitude of the COR polarization, thereby decreasing the COR-COR correlations. Above T_d , only the CDR-CDR radial contributions remain.

ACKNOWLEDGMENTS

The authors thank S. Gramsch and E. Venturini for their useful discussions. This work was sponsored by the Office of Naval Research under Grants No. N00014-07-1-0451 and No. N00014-02-1-0506 and the Carnegie/Department of Energy Alliance Center (CDAC, Grant No. DE-FC03-03NA00144). Use of the Advanced Photon Source was supported by the (U.S.) Department of Energy under Contract No. DE-AC02-06CH11357.

¹S. E. Park and T. R. ShROUT, *J. Appl. Phys.* **82**, 1804 (1997).

²G. A. Samara, *Phys. Rev. Lett.* **77**, 314 (1996).

³G. A. Samara, *Phys. Rev. B* **71**, 224108 (2005).

⁴G. Burns and F. H. Dacol, *Solid State Commun.* **48**, 853 (1983).

⁵I.-K. Jeong, T. W. Darling, J. K. Lee, T. Proffen, R. H. Heffner,

J. S. Park, K. S. Hong, W. Dmowski, and T. Egami, *Phys. Rev. Lett.* **94**, 147602 (2005).

⁶H. Hiraka, S.-H. Lee, P. M. Gehring, G. Xu, and G. Shirane, *Phys. Rev. B* **70**, 184105 (2004).

⁷G. Xu, Z. Zhong, H. Hiraka, and G. Shirane, *Phys. Rev. B* **70**,

- 174109 (2004).
- ⁸M. Ahart, R. E. Cohen, V. Struzhkin, E. Gregoryanz, D. Rytz, S. A. Prosandeev, H.-k. Mao, and R. J. Hemley, *Phys. Rev. B* **71**, 144102 (2005).
- ⁹P.-E. Janolin, B. Dkhil, P. Bouvier, J. Kreisel, and P. A. Thomas, *Phys. Rev. B* **73**, 094128 (2006).
- ¹⁰P. M. Gehring, H. Hiraka, C. Stock, S.-H. Lee, W. Chen, Z.-G. Ye, S. B. Vakhrushev, and Z. Chowdhuri, *Phys. Rev. B* **79**, 224109 (2009).
- ¹¹M. Paściak, M. Wołczyrz, and A. Pietraszko, *Phys. Rev. B* **76**, 014117 (2007).
- ¹²S. Vakhrushev, A. Ivanov, and J. Kulda, *Phys. Chem. Chem. Phys.* **7**, 2340 (2005).
- ¹³T. R. Welberry and D. J. Goossens, *Acta Crystallogr., Sect. A: Cryst. Phys., Diffr., Theor. Gen. Crystallogr.* **64**, 23 (2008).
- ¹⁴S. Tinte, B. P. Burton, E. Cockayne, and U. V. Waghmare, *Phys. Rev. Lett.* **97**, 137601 (2006).
- ¹⁵G. Xu, G. Shirane, J. R. D. Copley, and P. M. Gehring, *Phys. Rev. B* **69**, 064112 (2004).
- ¹⁶Y. Bing and Z. G. Ye, *J. Crystal Growth* **250**, 118 (2003).
- ¹⁷U. Rutt, M. A. Beno, J. Stempfer, G. Jennings, C. Krutz, and P. A. Montano, *Nucl. Instrum. Methods Phys. Res. A* **467-468**, 1026 (2001).
- ¹⁸Y. Feng, M. S. Somayazulu, R. Jaramillo, and T. F. Rosenbaum, *Rev. Sci. Instrum.* **76**, 063913 (2005).
- ¹⁹B. Dkhil, P. Gemeiner, A. Al-Barakaty, L. Bellaiche, E. Dul'kin, E. Mojaev, and M. Roth, *Phys. Rev. B* **80**, 064103 (2009).
- ²⁰S. Ravy, J.-P. Itie, A. Polian, and M. Hanfland, *Phys. Rev. Lett.* **99**, 117601 (2007).
- ²¹C. A. Randall, S. A. Markgraf, A. S. Bhalla, and K. Baba-Kishi, *Phys. Rev. B* **40**, 413 (1989).
- ²²U. V. Waghmare and K. M. Rabe, *Phys. Rev. B* **55**, 6161 (1997).
- ²³W. Zhong, D. Vanderbilt, and K. M. Rabe, *Phys. Rev. B* **52**, 6301 (1995).
- ²⁴B. P. Burton, E. Cockayne, and U. V. Waghmare, *Phys. Rev. B* **72**, 064113 (2005).
- ²⁵P. K. Davies and M. A. Akbas, *J. Phys. Chem. Solids* **61**, 159 (2000).
- ²⁶T. Egami and S. J. L. Billinge, *Underneath the Bragg Peaks: Structural Analysis of Complex Materials* (2003).
- ²⁷H. Krakauer, R. Yu, C.-Z. Wang, K. M. Rabe, and U. V. Waghmare, *J. Phys. Condens. Matter* **11**, 3779 (1999).